Journal of Physical Sciences, Vol. 23, 2018, 189-199
ISSN: 2350-0352 (print), www.vidyasagar.ac.in/publication/journal
Published on 24 December 2018

Structural and Electrical Studies of Nanocrystalline Fe_2O_3 Prepared by Microwave Assisted Solution Combustion Method with Mixed Fuel Approach

R. M. Belekar

Department of Physics and Electronics
Government Vidarbha Institute of Science and Humanities
Amravati, Maharashtra, India-444 604
Email: rajubelekar@gmail.com

Received 16 June 2018; accepted 11 December 2018

ABSTRACT

This research work comprises synthesis of haematite (Fe_2O_3) nanoparticles using microwave assisted sol gel auto combustion method using solution combustion reaction between ferric nitrate as oxidizer and a mixture of urea and glycine fuel as reducer. In this fuel mixture, urea was taken as stoichiometric fuel and glycine was added as excess fuel to alter the exothermic properties of redox reaction between ferric nitrate and urea. The synthesized powder were characterized by XRD, FT-IR, TGA-DTA showing that the powders were composed of polycrystalline oxides with crystallite size of 30 nm with gamma Fe_2O_3 phase without sintering. The phase transition from gamma Fe_2O_3 to alpha haematite occurs at temperature of 482˚C. The curie temperature was calculated from Gouy's balance and found to be 250 K. The electrical conductivity of nano Fe_2O_3 in pellet form was studied by impedance analyser at different temperature and frequencies. The variation of dielectric constant, ac conductivity with temperature and frequencies was also studied.

Keywords: Nanomaterials, Haematite, Mixed fuel approach, electrical conductivity.

1. Introduction

Iron oxide is one of the transition metal oxide that commonly exists in three phases in nature: maghemite (γ-Fe_2O_3), magnetite (Fe_3O_4) and haematite (α-Fe_2O_3). These materials find vide applications in various fields because of their catalytic activity, biocompatibility, low-cost, nontoxicity and environmentally friendly nature [15,6]. Fe_2O_3, the iron oxide has four crystallographic phases, namely maghemite (γ-Fe_2O_3), haematite (α-Fe_2O_3), maghemite (γ-Fe_2O_3), β-Fe_2O_3 and ε-Fe_2O_3 [21]. Out of which haematite is the thermodynamically stable phase of Fe2O3, and it is the subject of this current research work. Haematite happens to be exists in the rhombohedral crystal system with n-type semiconducting properties [30]. Iron oxide (α-Fe_2O_3) has been studied in various fields, including applications in photocatalysis [3,13,14,22], pigments [7], gas sensors [10], solar cells [25], and lithium ion batteries [20]. The γ-Fe_2O_3 undergoes a transformation to α-Fe_2O_3 above a transformation temperature (T_t) (reported to be of 500°C for γ-Fe_2O_3 NPs.

There is a homogeneous dispersion of nanoscale materials inside bulk thermoelectric matrices [9].The heat of transport/storage of materials is determined by phonons characteristics like frequency, scattering, velocity etc [31]. The boundaries of nanoparticles can acts as scattering centers for phonons transport which reduces their mean free path [8]. The result of which is reduction in its lattice thermal conductivity of nanomaterial. Thus the thermal conductivity of materials is reduced to improve their electric and magnetic properties for thermo-electric and thermo-magnetic applications. Because of low electrical conductivity, the electrical and chemical stability of nano scale material are also enhanced.

There are many chemical processes available for the synthesis of nanomaterials, out of which self-sustaining solution combustion synthesis is convenient in process, simple in experimental device and time saving. In solution combustion synthesis method, an aqueous mixture containing suitable metal salts which are the precursors of the final desired oxide and a proper sacrificial organic fuel which acts as reagent reducer. In this method, hydrated nitrates are generally preferred to other salts because of their good solubility in water which allows them to obtain a highly homogeneous solution. Depending upon the combustion temperature required, the fuel can be chosen. The nitrogen rich fuel produced higher heat whereas carbon rich fuel produces comparatively lower heat. The amount of heat required can be optimized by selecting proper mixture of the fuel. Urea is the most convenient fuel that can be used in the combustion processes [28] because of its relatively low price, availability, commercially grade and safety. In this study, haematite (Fe_2O_3) nanoparticles were synthesized using sol gel auto combustion method using solution combustion reaction between ferric nitrate as oxidizer and a mixture of urea and glycine fuel as reducer. The synthesized powder will be characterized by XRD, FT-IR, TGA-DTA and electrical and magnetic studies will also be conducted.

2. Experimental

The precursor involved in this synthesis is ferric nitrate ($Fe(NO_3)_3 \cdot 9H_2O$) from Merck (AR Grade). Urea $CO(NH_2)_2$ and glycine ($C_2H_5NO_2$) are used as fuel because of its relatively low price, availability, commercially grade and safety. The stoichiometric quantities of the oxidizers ($Fe(NO_3)_3 \cdot 9H_2O$) and fuels (Urea and glycine) were mixed in 50 ml deionized water with constant stirring. In this reaction urea was taken as stoichiometric fuel and glycine was added as excess fuel to alter the exothermicity of redox reaction between ferric nitrate and urea. This homogeneous solution was then kept on hot plate in order to evaporate more than half of water content and form gel like liquid. This solution moved to microwave with power of 900 Watt. After few minutes, first a gel-like structure was obtained and then swelled, followed by the evolution of a large volume of gases and self-propagating solution combustion reaction occurred. This reaction product was treated at temperature of 500˚C to obtain desired phase of Fe_2O_3. The identification and phase determination of the compound were done by powder XRD technique and other characterization was also being done with FT-IR, TGA-DTA.

For the preparation of pellets, all the compounds are grinded separately to fine particles in an agate mortar. The powder is then mixed with solution of 5% polyvinyl acetate (PVA) in A.R. grade acetone, which serves as a binder. About 2ml of binder per gram of powder is sufficient to give well-molded pellets. The plastic mass formed by mixing binder in the powdered sample is then pressed in a hydraulic press under a

pressure of 50-tones/sq. inch for about fifteen minutes. The pellets so formed are heated in a furnace up to 400^{o}C for about 3 hour to remove the binder. The furnace is then cooled to the room temperature by a natural way to obtain crack and moisture free hard pellets. The end faces of pellets are gently grinded with acetone to ensure its smooth face. After formation of pellets, a thin layer of silver paste is applied on both the surfaces of the pellets to provide good electrical contacts. The contacts are dried up to obtained a thin layer of silver which is adherent and chemically inert. The contacts are conformed, before the experimental study. The dimensions of pellets are measured accurately using digital vernier calliper.[2]

3. Results and discussion

The prepared samples of Fe_2O_3 were examined with the help of X ray diffraction technique in order to study the haematite phase and to determine particle size. Figure 1 shows the x-ray diffraction (XRD) peak lines from the standard order diffraction files of α-Fe_2O_3 (33–0664), and γ-Fe_2O_3 (39–1346), and it can be found that γ-Fe_2O_3 has a crystal structure similar to that of Fe_3O_4. [11] It is noteworthy that the annealing treatment is a key step in most synthesis of different crystalline phase of iron oxides. Any type of iron oxide can be obtained from the other types by oxidizing or reducing in the annealing treatment. It is also clear that the annealing temperature was not sufficient to turn γ-Fe_2O_3 into α-Fe_2O_3, as some unidentified peaks appeared in Xray diffractogram.[29]

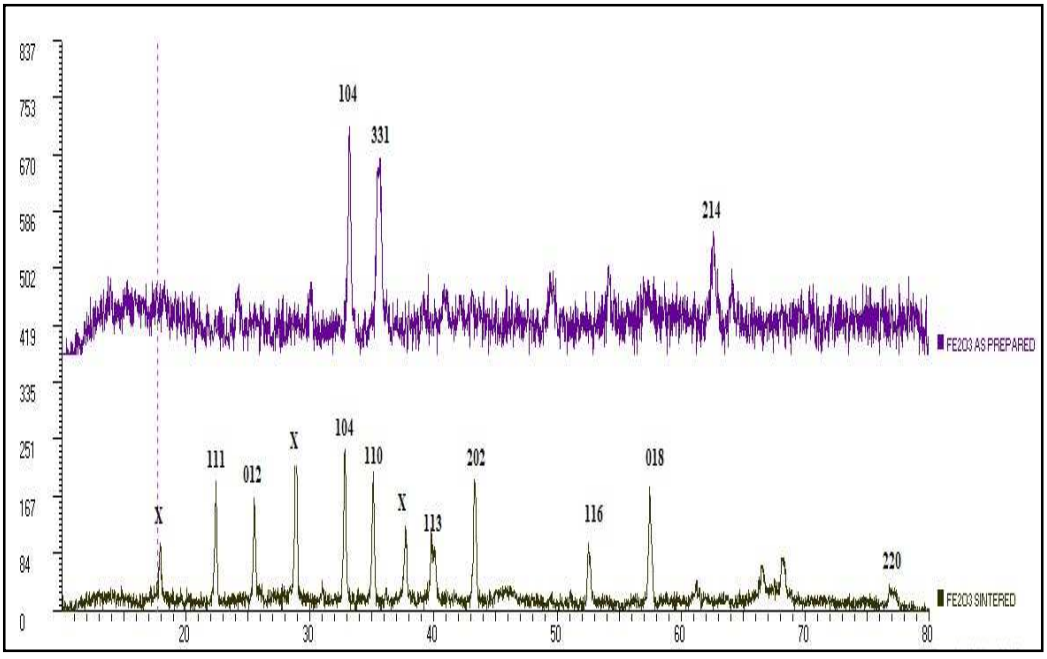

Figure 1: XRD diffractogram of nano Fe_2O_3 as prepared and sintered sample with JCPDS Card No. 39-1346 and 33-0664 respectively.

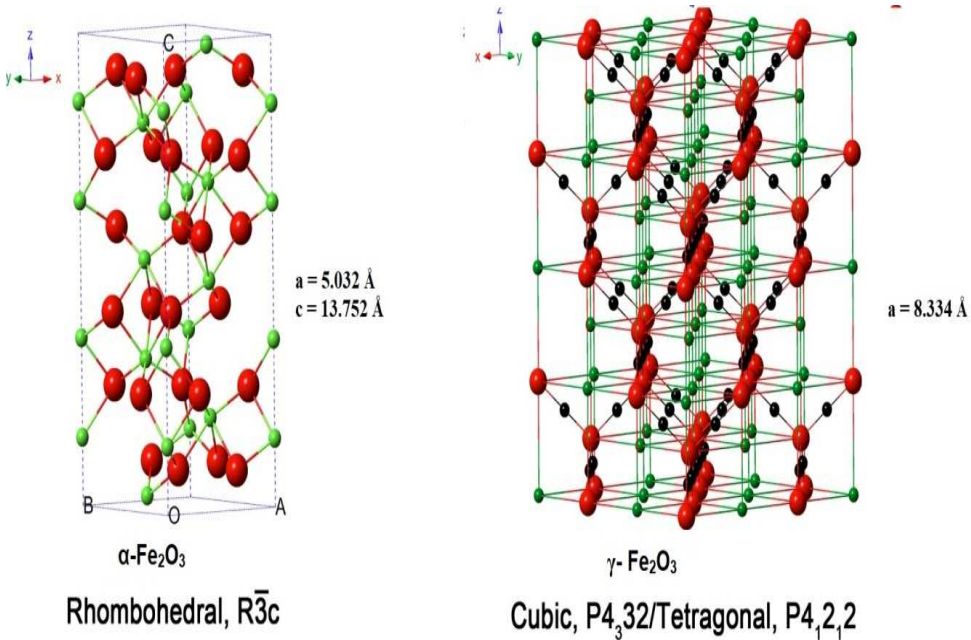

Figure 2: Crystal Structure of nano Fe_2O_3 in rhombohedral and cubic form.

As shown in figure 2, the structure of γ-Fe_2O_3 is cubic; each unit of γ-Fe_2O_3 contains 32 O^{2-} ions, 21⅓ Fe^{3+} ions and 2⅓ vacancies. Oxygen anions give rise to a cubic close-packed array while ferric ions are distributed over tetrahedral sites (eight Fe ions per unit cell) and octahedral sites (the remaining Fe ions and vacancies). Therefore, γ-Fe_2O_3 can be considered as fully oxidized magnetite, and it is an n-type semiconductor with a bandgap of 2.0 eV. α-Fe_2O_3 is an n-type semiconductor with a band gap of 2.3 eV, where the conduction band (CB) is composed of empty d-orbitals of Fe^{3+} and the valence band (VB) consists of an occupied 3d crystal field orbitals of Fe^{3+} in addition with some admixture from the O 2p non-bonding orbitals. As shown in figure 2, Fe^{3+} ions occupy two-thirds of the octahedral sites that are confined by the nearly ideal hexagonal close-packed O lattice.

The infrared spectra of the as-synthesized precursor a sample before thermal treatment and after thermal treatment at 500˚C is shown in figure 3. The prominent bands at 602 $cm^{-1}$and 465 cm^{-1} observed in the spectrum (Fig. 3) which can be attributed to Fe-O vibrational modes.[4,17,34]. The peak observed at 1670 cm^{-1} attributed to O-H bending vibrational modes. [1,27]. This strong band may also be due to physically adsorbed water. Although the O–H bond vibration around 3000 cm^{-1} is still present, the intensity of this band decreased markedly on heating the samples at 500˚C**.**The prominent band at 1031 cm^{-1} can be assigned to the absorption of –C-O-C bonds. The band at 1370 cm^{-1} may be attributed to –C-O stretching mode. [24] Absorption at 1409 cm^{-1} should be attributed to C-H vibration of the hydrolyzed products.

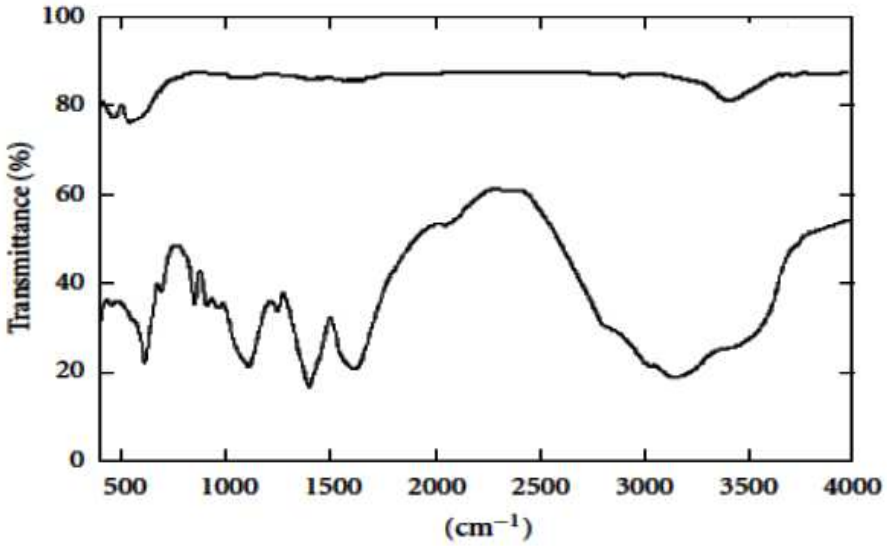

Figure 3: FT-IR spectrum of nano Fe_2O_3 as prepared and treated at 500˚C.

The temperature dependence of magnetic susceptibility measurement was done by using Gouy's Balance method. In Gouy's method, the sample of magnetic material suspended in a magnetic field and Gouy's balance measures the apparent changes in the mass of ferromagnetic sample as it is repelled or attracted by the region of magnetic field between the poles. The plots of the inverse of magnetic susceptibility ($1/\chi$) versus temperature for $\boldsymbol{Fe_2O_3}$ samples are shown in **Fig. 4**. The value of inverse of magnetic susceptibility ($1/\chi$) found to be increases with enhancement in temperature, in the ferromagnetic region followed by a sudden increase at the certain temperature indicating transition to the paramagnetic region. The temperature at which the magnetic transition occurs is known as the Curie temperature (T_c). The magnitude of Curie temperature (T_c) was calculated by extrapolating the paramagnetic region to the X-axis. Low temperature magnetic transition occurs at 250 K (Morin temperature). At temperature $T \leq 250$ K: The magnetic arrangement has Fe^{3+} spins directed along the [111] axis and paired across the shared octahedral face. At $T \geq 250$ K: The spins become essentially localized in (111) sheets directed towards the three nearest neighbours. However, it was observed that, the spins have canted slightly out of the plane, giving rise to a weak ferromagnetic moment along the [111] axis.

The relationship between conductivity and temperature may be expressed as by the relation [32],

$$\sigma = \sigma_0 \exp\left(\Delta E / KT\right) \quad (1)$$

where, σ is the conductivity, T is the temperature, K is the Boltzmann constant, and ΔE is the activation energy, is the energy required to jump an electron to neighboring ion, so giving rise to electrical conductivity. The conductivity is measured by taking sample in the pellet form by Precision Impedance Analyzers 6500B Series.

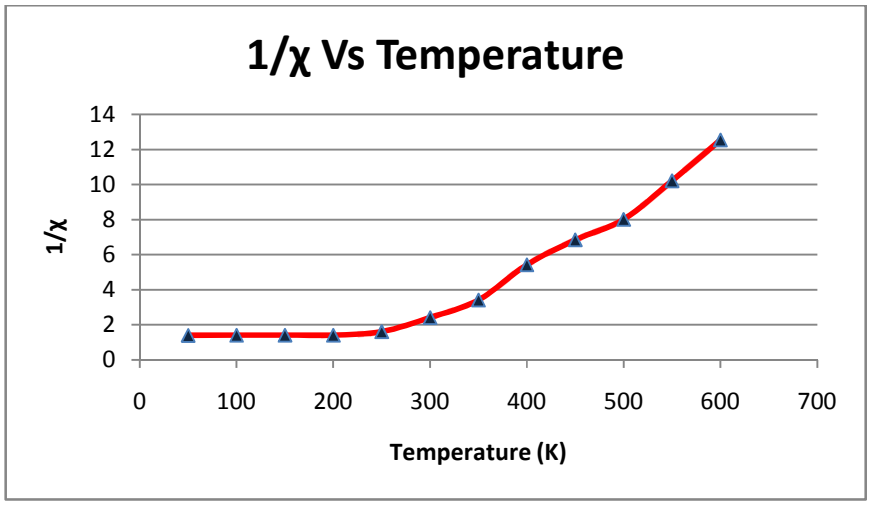

Figure 4: Plot of inverse susceptibility versus temperature.

Generally the Fe_2O_3 are insulator at room temperature and act as a semiconductor under the influence of high temperature. The electrical conduction in Fe_2O_3 is a combination of electronic and ionic conduction such that conduction at low temperatures is dominated by electrons whereas at high temperature it is dominated by ionic hopping mechanism [18].

The electrical properties of the ferrite can be understood from the measurement of electrical conductivity, dielectric behaviour, thermoelectric power, etc. The mobility of charge carriers are the key quantities for obtaining inner details of conductivity. The low conductivity of ferrite greatly influences the various applications at microwave frequencies. The ferrite and ferroelectric can have their own electrical properties but their composites with different substitutions of divalent, trivalent and tetravalent ions are designed to give more effective property. Though ferrites are semiconductors at high temperature, the conduction mechanism is quite different than that of semiconductors. In ferrites the carrier concentration is almost constant but mobility of carriers is affected by temperature. Thus, the conduction in ferrites can be explained in terms of polaron hopping process and there are experimental evidences for the existence of polarons and its hopping [16,19].

The plots of log conductivity (σ) with inverse of temperature for Fe_2O_3 are shown in fig.5. From these plots it can be seen that the conductivity increase slowly up to a certain temperature called as transition temperature (T_t), where there is a slight change in slope occur after which a rapid increase is obtained. Above the transition temperature, the synthesized ferrite samples exhibit paramagnetic nature where it has disordered character.

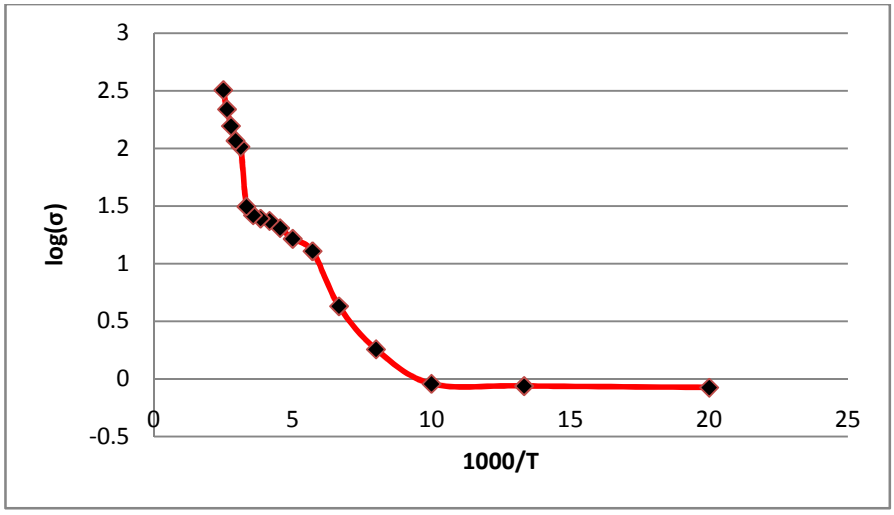

Figure 5: Plot of log(σ) versus 1000/T for Fe_2O_3 pellet

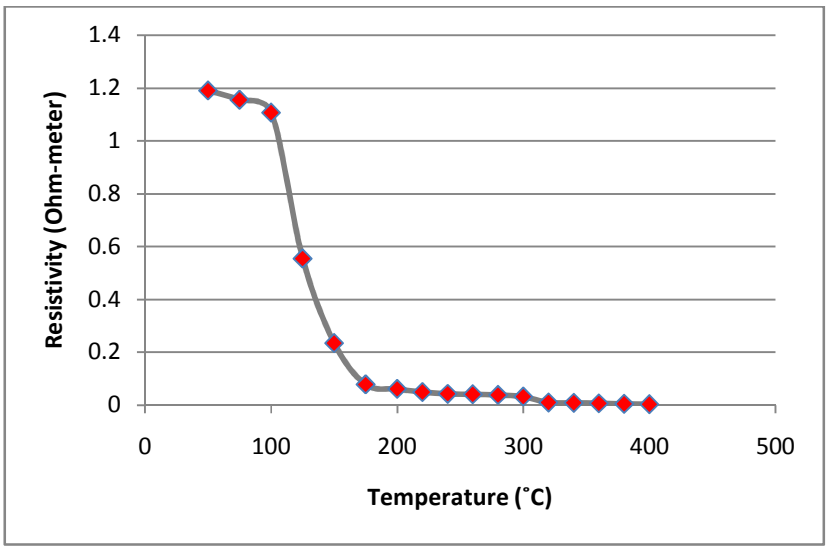

Figure 6: Plot of resistivity (in ohm-meter) versus temperature.

The electrical conductivity in ferrite is mainly due to hopping of electrons between ions of the same element present in more than one oxidation state, distributed randomly over crystallographically equivalent lattice sites. As the temperature is increased from 150 to 500˚C, one can see that the electrical resistivity decreases linearly as shown in figure 6, with an activation energy of 1.68 x 10^{-19} J (1.05 eV). Note that the conductivity at 500˚C is higher than that of RT by about three orders of magnitude and by six orders of magnitude as compared with that at about 150˚C.

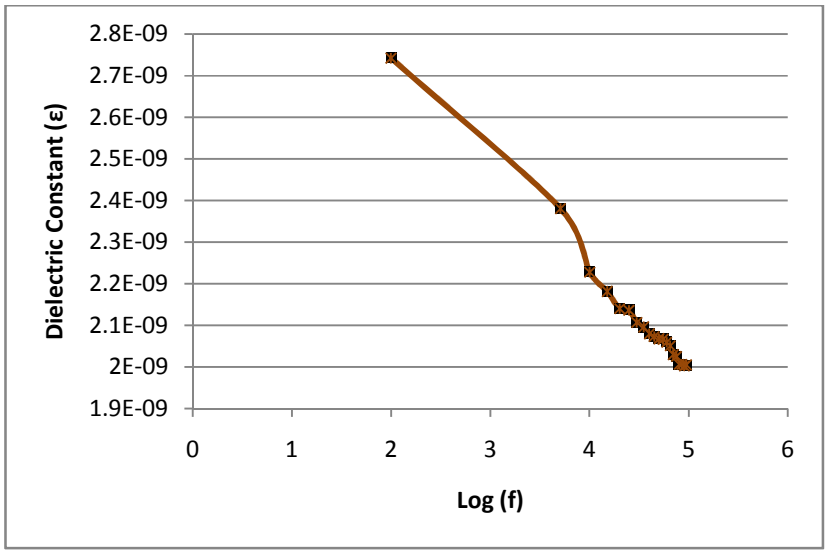

Figure 7: Plot of dielectric constant versus log of frequency.

The variation of dielectric constant with frequency for Fe_2O_3 is shown in the figure 7. It is seen that, the synthesized sample show frequency dependent phenomena i.e. the dielectric constant decreases with increasing frequency and then reaches to constant value. It is observed that ε´ decrease with increasing the applied field frequency showing a normal dielectric behavior of ferrites, which exists in non-homogenous layered structure of ceramic materials as explained by Maxwell–Wagner's two-layer model [33]. According to this model, ferrites consist of perfectly conducting grains separated by insulating grain boundaries, which offer hindrance to the conduction process. Under the influence of an applied field, displacement of charge carriers takes place. If resistance of grain boundary is large, the charge carriers align themselves at the grain boundaries, resulting in the polarization of the dielectric medium that leads to a large dielectric constant. As the frequency increases, the increase in electrical resistance due to dopant substitution diminishes the probability of charge carriers to reach the grain boundaries. This disrupts the polarization buildup in material leading to decrease the dielectric constant at higher frequencies.

From figure 7, it is seen that έ decreases gradually with increasing f. Such a behavior was previously reported for different ferrites [12,23] and could be explained assuming that the dielectric constant έ and the conductivity have the same origin where the conduction occurs through the electron hopping between Fe^{2+} and Fe^{3+} ions on the octahedral sites. By increasing the frequency, the electron hopping cannot follow the electric field fluctuations causing the dielectric constant έ to decrease as we found experimentally. According to Koops's model [26] the dielectric constant at low frequency comes from the grain boundaries which have a high dielectric constant due to high resistivity at grains boundaries. At high frequency έ results from the grains which have a small dielectric constant due to low resistivity. The higher values of dielectric constant at low frequency are due to the voids, dislocations and other defects. High dielectric constant decreases the penetration depth of the electromagnetic waves by increasing the

skin effect. Hence, the much lower dielectric constants obtained for the ferrites warrant their application at high frequencies [5].

4. Conclusion

The nano Fe_2O_3 sample was successfully prepared by simple solution combustion synthesis method using the precursors iron nitrate with mixed fuel approach. The structure and phase determination was carried out by XRD analysis. The Xray diffraction of as prepared sample has shown cubic structure indicating amorphous γ-Fe_2O_3 phase with average crystalline size of 32 nm calculated from Scherrer formula. When the sample is treated at some elevated temperature of 500˚C, γ-Fe_2O_3 is converted into thermodynamically stable α-Fe_2O_3 as indicated by XRD. The sharp peaks in the in XRD of sintered sample indicated crystalline nature of α-Fe_2O_3. When the sample is prepared by solution combustion synthesis it requires less temperature to form stable alpha phase (α-Fe_2O_3). The structural formation of ferrite was also confirmed by FTIR Spectra, showing band ranges 602 $cm^{-1}$and 465 cm^{-1} corresponding to Fe-O vibrations. It is also clear that if one wishes to obtain γ-Fe2O3 by calcination of the γ-FeOOH gel, annealing at lower temperature must be employed. The temperature dependence of electrical conductivity shows that the electrical conductivity of sintered Fe_2O_3 at 500 ˚C is three orders of magnitude higher than that of RT. In addition, the dominant charge carriers are found to be holes in the range between RT and 380˚C, while electrons above 380˚C according to the Seebeck measurement. The combine inductive and capacitive nature in the composites a promising candidate for design simplification and size minimization of many passive electronic devices such as integrated filters and microwave absorber. The ac conductivity of composites increases with increase in frequency, this is due to hopping of charge carriers amongst localized sites. The relative susceptibility gradually increases up to blocking temperature, suggestive of single domain (SD) existence in majority in ferrite phase.

Acknowledgment. The authors are thankful to Dr. Sanjay Mahajani (IIT, Powai) for providing lab facility and instrumentations to carry out above work.

The author is thankful to the reviewers for their suggestions towards betterment of the paper.

REFERENCES

1. S.K.Apte, S.D.Naik, R.S.Sonawane and B.B.Kalew, Synthesis of Nanosize□Necked Structure α□ and γ□Fe_2O_3 and its Photocatalytic Activity, Journal of American Ceramic Society, 90 (2007) 412–414.
2. R.M.Belekar, P.S.Sawadh, B.A.Shingade and G.C.Wakde, Synthesis, characterization and thermo-luminescence studies of carbon doped alumina prepared by conventional method, Advance and Innovative Research, 4(4) (2017) 166.
3. W.Chang, M. Zhang, X.Ren and A.Miller, Synthesis and photocatalytic activity of monolithic Fe_2O_3/TiO_2, South African Journal of Chemistry, 70 (2017) 127-131.
4. E.Darezereshki, One-Step Synthesis of Hematite (α-Fe2O3) Nano-Particles by Direct Thermal-Decomposition of Maghemite, Material Letters, 65 (2011) 642–645.

5. V.N.Dhage, M.L.Mane, A.P.Kecha, C.T.Birajdar and K.M.Jadhav, Structural and magnetic behaviour of aluminium doped barium hexaferrite nanoparticles synthesized by solution combustion technique, Physica B 406 (2011) 789-793.
6. S.M.El-Sheikh, F.A.Harraz, and K.A.Saad, Catalytic performance of nanostructured iron oxides synthesized by thermal decomposition technique, Journal of Alloys Compounds, 487, (2009) 716–723.
7. L.Frolova, A.Pivovarov and T.Butyrina, Synthesis of pigments in Fe_2O_3-Al_2O_3-CoO by co-precipitation method, Pigment & Resin Technology, 46 (5) (2017) 356-361.
8. A.Jeżowski, J.Mucha, R.Pazik and W.Strek, Influence of crystallite size on the thermal conductivity in $BaTiO_3$ nanoceramics, Applied Physics Letters, 90 (2007) 114104-7.
9. W. Kim, Strategies for engineering phonon transport in thermo-electrics, Journal of Material Chemistry C, 3 (2015) 10336-48.
10. H.C.Manh, H.N.Duc, V.D.Nguyen, V.T.Nguyen, L.D.T.Thanh and V.H.Nguyen, Synthesis and gas-sensing characteristics of α-Fe2O3 hollow balls, Journal of Science: Advanced Materials and Devices, 1(1) (2016) 45-50.
11. G.Martínez, A.Malumbres, R.Mallada, J.Hueso, S.Irusta, O.Bomatí-Miguel and Santamaría, Use of a polyol liquid collection medium to obtain ultrasmall magnetic nanoparticles by laser pyrolysis, Journal of Nanotechnology, 23 (2012) 425605.
12. J.C.Maxwell, Electricity and Magnetism, Vol.1, Oxford University Press, Oxford, Section 328 (1929).
13. M.Mishra and D.M.Chun, Fe_2O_3 as photocatalytic material: A review, Applied Catalysis A: General, Volume 498 (2015) 126-141.
14. T.Mishra, P.Mohapatra and K.M. Parida, Synthesis, characterisation and catalytic evaluation of iron–manganese mixed oxide pillared clay for VOC decomposition reaction, Applied Catalysis B: Environmental, 79(3) (2008) 279-285
15. G.K.Mor, H.E.Prakasam, O.K.Varghese, K.Shankar and C.A.Grimes, Vertically Oriented Ti−Fe−O Nanotube Array Films: Toward a Useful Material Architecture for Solar Spectrum Water Photoelectrolysis, Nano Letters 7, (2007) 2356–2364.
16. S.Murugavel and M.Upadhyay, A.C. Conduction in Amorphous Semiconductors, Journal of the Indian Institute of Science, 91(2) (2011) 303-317.
17. B.Pal and M.Sharon, Preparation of iron oxide thin film by metal organic deposition from Fe(III)-acetylacetonate: a study of photocatalytic properties, Thin Solid Films, 379 (2000) 83-88.
18. M.V.Patrakeev, E.B.Mitberg, I.A.Leonidov and V.L.Kozhevnikov, Electrical characterization of the intergrowth ferrite $Sr_4Fe_6O_{13+\delta}$, Solid State Ionics, 139 (2001) 325–330.
19. O. Prakash, K.D.Mandal, C.C.Christopher, M.S.Sastry and D. Kumar, Electrical behaviour of lanthanum- and cobalt-doped strontium stannate, Bulletin of Material Science,17 (1994) 253-257.
20. M.V.Reddy, T.Yu, C.H.Sow, Z.X.Shen, C.T.Lim, G.V.Subba Rao and B.V.R. Chowdari,α□Fe_2O_3 Nanoflakes as an Anode Material for Li□Ion Batteries, Advanced Functional Materials, 17 (2007) 2792 – 2799.

21. S.Sakurai, A.Namai, K.Hashimoto and S.Ohkoshi, First Observation of Phase Transformation of All Four Fe_2O_3 Phases ($\gamma \rightarrow \varepsilon \rightarrow \beta \rightarrow \alpha$-Phase), Journal of American Chemical Society, 131 (2009) 18299–18303.
22. N.N.Sarkar, K.G.Rewatkar, V.M.Nanoti, N.T.Tayade, and D.S.Bhowmick,
23. Structural and Magnetic Study of Zr^{4+} Substituted Magnesium Ferrite Nano-particles, Journal of Physical Sciences, 22 (2017) 107-113.
24. A. Sathiya Priya, D.Geetha and N.Kavitha, Evaluation of structural and dielectric properties of Al, Ce co-doped cobalt ferrites, Materials Research Express,5 (6) (2018) 066109.
25. S.S.Shankar, A.Rai, A.Ahmad and M.Sastry, Rapid synthesis of Au, Ag and bimetallic Au core-Ag shell nanoparticles using Neem (Azadirachta indica) leaf broth, Journal of Colloid Interface Science, 275 (2004) 496–502.
26. S.S.Shinde, R.A.Bansode, C.H.Bhosale and K.Y.Rajpure, Physical properties of hematite α-Fe2O3 thin films: application to photo-electrochemical solar cells, Journal of Semiconductors, 32 (1) (2011) 013001.
27. A.Singh, S.B.Narang, K.Singh, P.Sharma and O.P.Pandey, Structural, AC conductivity and dielectric properties of Sr-La hexaferrite. European Physical Journal-applied Physics, 33(3) (2006) 189-193.
28. L.Song, S.Zhang, B.Chen, J.Ge and X.Jia, A hydrothermal method for preparation of α-Fe_2O_3nanotubes and their catalytic performance for thermal decomposition of ammonium perchlorate, Colloids and Surfaces A: Physicochemical and Engineering Aspects, 360 (2010) 1–5.
29. K.Tahmasebi and M.Paydar, The effect of starch addition on solution combustion synthesis of Al_2O_3-ZrO_2 nanocomposite using urea as a fuel, Journal of Materials Chemistry and Physics, 109 (2008)156-163.
30. N.T.Tayade, S.Dhawankar and P.R.Arjuwadkar, Perspective of Distortion and Vulnerability in Structure by Using the CdS-ZnS Composite Approach in Rietveld Refinement, Journal of Physical Sciences, Vol. 22 (2017) 137-150.
31. A.S.Teja and P.Y.Koh, Synthesis, properties, and applications of magnetic iron oxide nanoparticles, Progress in Crystal Growth and Characterisation of Materials,55 (2009) 22–45.
32. E.S.Toberer, L.L.Baranowski, and C.Dames, Advances in thermal conductivity Annual Review Material Research, 42 (2012)179-209.
33. E.J.W.Verwey and E.L.Heilman, Physical properties and cation arrangement of oxides with spinel structures I. Cation arrangement in spinels, Journal of Chemical Physics, 15 (1947) 174.
34. T.T.N.Vu, G.Teyssedre, S.L.Roy and C.Lauren, Maxwell–Wagner Effect in Multi-Layered Dielectrics: Interfacial Charge Measurement and Modelling, Technologies 5 (27) (2017) 1-15.
35. Y.Y.Xu, D.Zhao, X.J.Zhang, W.T.Jin, P.Kashkarov and H.Zhang, Synthesis and characterization of single crystalline α-Fe2O3 nanoleaves, Physica E, 41(2009) 806–811